Image quality and geometric distortion of modern diffusion-weighted imaging sequences in magnetic resonance imaging of the prostate

Stocker, Daniel ; Manoliu, Andrei ; Becker, Anton S ; Barth, Borna K ; Nanz, Daniel ; Klarhöfer, Markus ; Donati, Olivio F

Abstract: PURPOSE: The aim of this study was to compare qualitative and quantitative image quality and geometric distortion of 4 magnetic resonance diffusion-weighted imaging (DWI) sequences of the prostate using comparable imaging parameters and similar acquisition times. METHODS AND MATERIALS: Axial T2-weighted turbo spin echo images and axial DWI echo-planar imaging (EPI) sequences, including single-shot spin-echo (ss-EPI), readout-segmented multishot (rs-EPI), selective excitation-reduced field of view (sTX-EPI), and prototype single-shot technique applying slice-specific shimming (iShim-EPI) sequences, were acquired at 3 T in 10 healthy volunteers (mean age, 26.1 ± 3.8 years; body mass index, 23.2 ± 3.0 kg/m). Two radiologists, blinded to the type of DWI, independently rated DWIs on a 5-point Likert scale regarding subjective image quality features (resolution, demarcation of prostate capsule, zonal anatomy). Interreader agreement was assessed using the intraclass correlation coefficient. Signal-to-noise ratio (SNR) and apparent diffusion coefficient (ADC) values were assessed separately in the peripheral and transitional zone. For the analysis of geometric distortion, the diameter of the prostate from left to right and from anterior to posterior was measured at the level of the verumontanum on b-1000 DWIs and on T2-weighted turbo spin echo images. Differences were compared using the Wilcoxon rank sum test for qualitative parameters, analysis of variance, and Friedman test for quantitative parameters. A P value of less than 0.05 was considered significant, with correction for multiple comparisons. RESULTS: Interreader agreement was good to excellent (intraclass correlation coefficient, 0.71-0.79) for all qualitative features. Subjective image quality regarding "resolution" was significantly better for ss-EPI than rs-EPI (mean Likert score, 4.25 vs 3.8; P = 0.031) and sTX-EPI (4.25 vs 3.3; P = 0.046) and for iShim-EPI as compared with rs-EPI (4.4 vs 3.8; P = 0.031) and sTX-EPI (4.4 vs 3.3; P = 0.047). There was no significant difference regarding capsule demarcation and zonal anatomy. Signal-to-noise ratio was significantly higher in iShim-EPI than sTX-EPI (SNR ± standard deviation [SD], 28.13 ± 8.21 vs 14.96 ± 2.4; P = 0.015). The ADC values were lower for the peripheral zone in the sTX-EPI than in the ss-EPI (ADC ± SD, 1002.94 ± 83.51 vs 1165.05 ± 115.64; P = 0.013) and the rs-EPI (1002.94 ± 83.51 vs 1244.40 ± 89.95; P = 0.0012) and in the transitional zone in the sTX-EPI compared with the rs-EPI (874.50 ± 200.72 vs 1261.47 ± 179.23; P = 0.0021). There were no statistically significant differences in geometric distortion between all DWI sequences. CONCLUSIONS: Single-shot spin-echo EPI and iShim-EPI showed a tendency toward superior image quality and SNR compared with rs-EPI and sTX-EPI with no significant differences in geometric distortion.

DOI: https://doi.org/10.1097/RLI.0000000000000429

Originally published at:
Stocker, Daniel; Manoliu, Andrei; Becker, Anton S; Barth, Borna K; Nanz, Daniel; Klarhöfer, Markus; Donati, Olivio F (2018). Image quality and geometric distortion of modern diffusion-weighted imaging sequences in magnetic resonance imaging of the prostate. Investigative Radiology, 53(4):200-206.
DOI: https://doi.org/10.1097/RLI.0000000000000429

Image Quality and Geometric Distortion of Modern Diffusion-Weighted Imaging Sequences in Magnetic Resonance Imaging of the Prostate

Daniel Stocker, MD, Andrei Manoliu, MD, PhD,* Anton S. Becker, MD,* Borna K. Barth, MD,* Daniel Nanz, PhD,* Markus Klarhöfer, PhD,† and Olivio F. Donati, MD**

Purpose: The aim of this study was to compare qualitative and quantitative image quality and geometric distortion of 4 magnetic resonance diffusion-weighted imaging (DWI) sequences of the prostate using comparable imaging parameters and similar acquisition times.

Methods and Materials: Axial T2-weighted turbo spin echo images and axial DWI echo-planar imaging (EPI) sequences, including single-shot spin-echo (ss-EPI), readout-segmented multishot (rs-EPI), selective excitation–reduced field of view (sTX-EPI), and prototype single-shot technique applying slice-specific shimming (iShim-EPI) sequences, were acquired at 3 T in 10 healthy volunteers (mean age, 26.1 ± 3.8 years; body mass index, 23.2 ± 3.0 kg/m^2). Two radiologists, blinded to the type of DWI, independently rated DWIs on a 5-point Likert scale regarding subjective image quality features (resolution, demarcation of prostate capsule, zonal anatomy). Interreader agreement was assessed using the intraclass correlation coefficient. Signal-to-noise ratio (SNR) and apparent diffusion coefficient (ADC) values were assessed separately in the peripheral and transitional zone. For the analysis of geometric distortion, the diameter of the prostate from left to right and from anterior to posterior was measured at the level of the verumontanum on b-1000 DWIs and on T2-weighted turbo spin echo images. Differences were compared using the Wilcoxon rank sum test for qualitative parameters, analysis of variance, and Friedman test for quantitative parameters. A P value of less than 0.05 was considered significant, with correction for multiple comparisons.

Results: Interreader agreement was good to excellent (intraclass correlation coefficient, 0.71–0.79) for all qualitative features. Subjective image quality regarding "resolution" was significantly better for ss-EPI than rs-EPI (mean Likert score, 4.25 vs 3.8; $P = 0.031$) and sTX-EPI (4.25 vs 3.3; $P = 0.046$) and for iShim-EPI as compared with rs-EPI (4.4 vs 3.8; $P = 0.031$) and sTX-EPI (4.4 vs 3.3; $P = 0.047$). There was no significant difference regarding capsule demarcation and zonal anatomy. Signal-to-noise ratio was significantly higher in iShim-EPI than sTX-EPI (SNR ± standard deviation [SD], 28.13 ± 8.21 vs 14.96 ± 2.4; $P = 0.015$). The ADC values were lower for the peripheral zone in the sTX-EPI than in the ss-EPI (ADC ± SD, 1002.94 ± 83.51 vs 1165.05 ± 115.64; $P = 0.013$) and the rs-EPI (1002.94 ± 83.51 vs 1244.40 ± 89.95; $P = 0.0012$) and in the transitional zone in the sTX-EPI compared with the rs-EPI (874.50 ± 200.72 vs 1261.47 ± 179.23; $P = 0.0021$). There were no statistically significant differences in geometric distortion between all DWI sequences.

Conclusions: Single-shot spin-echo EPI and iShim-EPI showed a tendency toward superior image quality and SNR compared with rs-EPI and sTX-EPI with no significant differences in geometric distortion.

Key Words: diffusion-weighted imaging, prostate, image quality, geometric distortion

(*Invest Radiol* 2017;00: 00–00)

Diffusion-weighted imaging (DWI) is an integral component of multiparameteric magnetic resonance imaging (MRI) of the prostate and is one of the key sequences for detection of prostate cancer.[1–3] Various DWI sequences have shown high diagnostic performance in prostate cancer detection and the ability to assess cancer aggressiveness.[4–6] Especially in higher field strength (3 T) imaging, the widely used single-shot spin-echo echo-planar imaging (ss-EPI) techniques are hampered by the presence of artifacts such as geometric distortion or susceptibility caused by B_0-field variations and off resonance effects.[7–9]

Recently, novel acquisition techniques have been introduced to diminish these artifacts and to improve image quality. Readout-segmented multishot EPI (rs-EPI) sequences allow for shorter echo-spacing in the EPI echo-train compared with regular ss-EPI DWI by sampling a smaller number of k_x points for each readout segment, leading to a reduction of T_2^* blurring effects and to a higher nominal resolution.[10] Selective excitation–reduced field of view (FOV) EPI (sTX-EPI) sequences reduce the size of the FOV along the phase-encoding direction by applying 2-dimensional (2D), spatial-selective excitation pulses. Thus, the length of the EPI echo-train is shortened, resulting in reduced geometric distortion and increased resolution.[11,12] Magnetic field inhomogeneities and geometric distortion can also be reduced by slice-selective optimization of the main magnetic field in combination with a standard EPI readout (prototype single-shot technique applying slice-specific shimming [iShim-EPI]).[13,14]

Recent studies have demonstrated improved image quality and reduced artifacts in prostate MRI for rs-EPI and sTX-EPI compared with ss-EPI.[12,15,16] Another study showed that iShim-EPI reduced the impact of susceptibility effects as well as improved signal intensity, spatial alignment and improved signal-to-noise ratio (SNR) in whole-body DWI compared with DWI using conventional shimming.[14] A comparison of all 4 DWI techniques, however, regarding image quality and geometric distortion in MRI of prostate cancer has not yet been performed. While a limited overall image quality may hamper the detection of prostate cancer foci, geometric distortion may not only influence quantitative apparent diffusion coefficient (ADC) values,[17] but may also impede accurate coregistration of sequences needed for radiation planning[18] or for MRI-guided targeted biopsies.

Thus, the purpose of this study was to compare qualitative and quantitative image quality and geometric distortion between ss-EPI, rs-EPI, sTX-EPI, and iShim-EPI DWI of the prostate using comparable imaging parameters for all sequences and especially similar acquisition times.

MATERIALS AND METHODS

This prospective study was approved by the regional ethics committee. Written informed consent was obtained from each volunteer.

Received for publication August 9, 2017; and accepted for publication, after revision, September 25, 2017.

From the *Institute of Diagnostic and Interventional Radiology, University Hospital Zurich, University of Zurich; and †Siemens Healthcare AG, Zurich, Switzerland.

Conflicts of interest and sources of funding: Markus Klarhöfer, PhD, is an employee of Siemens Healthcare AG, Zürich. All other authors declare that they have no conflict of interest.

Supplemental digital contents are available for this article. Direct URL citations appear in the printed text and are provided in the HTML and PDF versions of this article on the journal's Web site (www.investigativeradiology.com).

Correspondence to: Olivio F. Donati, MD, Institute of Diagnostic and Interventional Radiology, University Hospital Zurich, University of Zurich, Rämistrasse 100 CH-8091 Zurich, Switzerland. E-mail: olivio.donati@usz.ch.

ISSN: 0020-9996/17/0000–0000
DOI: 10.1097/RLI.0000000000000429

Study Population

Ten healthy volunteers without known pathology of the prostate underwent an adapted prostate MRI protocol between October 2015 and February 2016 at our department (mean age, 26.1 ± 3.8 years; body mass index, 23.2 ± 3.0 kg/m^2). Inclusion criteria were (1) age older than 18 years, (2) no contraindications for MR scanning, and (3) no known focal prostate lesion. No instructions with regards to clearing rectal gas were given before the MRI.

MRI Technique

We acquired all images on 3 T whole-body MRI systems (MAGNETOM Skyra; Siemens Healthcare, Erlangen, Germany) using 2 independent transmit channels (TimTX TrueShape; Siemens Healthcare). A 60-channel phased-array receive coil was used for signal reception. Two different scan protocols with different order of the DWI sequences were performed. T2-weighted turbo-spin echo (TSE-T2W) images were always acquired first.

Axial TSE-T2W sequences were acquired with repetition time (TR)/echo time (TE), 6650/96 milliseconds; FOV, 222 × 222 mm^2; slice thickness (ST), 3 mm; and in-plane resolution, 0.5 × 0.5 mm^2.

Diffusion-weighted imaging sequences were acquired with orientation and location identical to TSE-T2W images. Parameters such as b-values, TR, in-plane resolution, ST, and acquisition time were kept identical, where possible. Echo time and TR were set to "minimum."

The resulting acquisition parameters for ss-EPI were as follows: TR/TE, 4600/68 milliseconds; receiver bandwidth, 1526 Hz/pixel; b-values, 100, 500, and 1000 s/mm^2; FOV, 222 × 222 mm^2; ST, 3 mm; in-plane resolution, 1.8 × 1.8 mm^2; acquisition time, 05:42 minutes.

For rs-EPI acquisition, the parameters were as follows: TR/TE, 4620/57 milliseconds; receiver bandwidth, 863 Hz/pixel; b-values, 100, 500, and 1000 s/mm^2; FOV, 222 × 222 mm^2; ST, 3 mm; in-plane resolution, 1.8 × 1.8 mm^2; read-out segments, 7; acquisition time, 05:48 minutes.

The parameters chosen for sTX-EPI acquisition were as follows: TR/TE, 4700/62 milliseconds; receiver bandwidth, 1526 Hz/pixel; b-values, 100, 500, and 1000 s/mm^2; FOV, 99 × 222 mm^2; ST, 3 mm; in-plane resolution, 1.8 × 1.8 mm^2; acquisition time, 5:48 minutes.

Parameters for iShim-EPI acquisition were as follows: TR/TE, 4400/68 milliseconds; receiver bandwidth, 1526 Hz/pixel; b-values, 100, 500, and 1000 s/mm^2; FOV, 222 × 222 mm^2; ST, 3 mm; in-plane resolution, 1.8 × 1.8 mm^2; acquisition time, 05:46 minutes.

Apparent diffusion coefficient maps were calculated for each DWI sequence with a monoexponential fit based on the 3 measured b-values. Sequence parameters are summarized in Table 1.

Qualitative Image Analysis

The b-1000 DWIs of all volunteers were independently reviewed by 2 radiologists (B.K.B and A.S.B. initials blinded, both with 2 years of experience in interpreting prostate MRI). All data sets were arranged in random order and reviewed in 1 reading session. The anatomical region presented on the screen was limited so both readers were blinded to the type of DWI (eg, the reduced FOV of the sTX-EPI was not identifiable). Resolution, demarcation of prostate capsule, zonal anatomy, geometric distortion, and overall image quality were assessed on a 5-point Likert scale (1, poor; 2, below average; 3, average; 4, above average; 5, excellent; 1, no distortion; 2, low distortion; 3, intermediate distortion; 4, high distortion; 5, very high distortion, respectively). "Resolution" was defined as the ability to recognize detailed anatomical structures within the prostate (urethra, verumontanum, etc). "Demarcation of the prostate capsule" was defined as ability to depict the prostatic capsule in a continuous fashion around the prostate. "Zonal anatomy" was defined to distinguish the transitional zone of the prostate from the peripheral zone. Furthermore, presence of artifacts (wrapping, ghosting, susceptibility, blurring, and other) and their influence on image quality were assessed on a 5-point Likert scale (1, no influence; 2, low influence; 3, moderate influence; 4, severe influence; 5, substantial influence, respectively). At the end of the session, the 4 DWI series for each patient were presented to the reader side-by-side, and they were asked to choose their overall preferred sequence.

Quantitative Image Analysis

SNR Measurements and Analysis

Signal-to-noise ratio analysis was performed according to an approach recently again described by Reeder and colleagues,[19] which has since been applied for SNR evaluation of different DWI/DTI sequences.[20,21] b-100 sequences in all diffusion sequences were acquired twice, and subtraction images for all sequences were calculated, resulting in 1 noise map for each set of sequences. Signal-to-noise ratio was calculated as follows:

$$SNR = \frac{|\rho|}{\sigma} \times \sqrt{2}$$

where ρ is the measured image intensity, proportional to the magnitude of the measured transverse magnetization; σ is the standard deviation of the corresponding noise components as measured on the difference image; and $\sqrt{2}$ is a correction factor.[20,21] First, voxel-wise SNR maps were calculated. In particular, both image data and corresponding noise data were postprocessed separately, resulting in voxel-based SNR maps.

TABLE 1. Magnetic Resonance Sequence Parameters for the 4 Different DWI Sequences

	ss-EPI	rs-EPI	sTX-EPI	iShim-EPI
b-value, s/mm^2	100, 500, 1000	100, 500, 1000	100, 500, 1000	100, 500, 1000
Averages	2, 6, 15	1, 1, 2	2, 6, 15	2, 6, 15
TR, ms	4600	4620	4700	4400
Minimum TE, ms	68	57	62	68
Matrix	126 × 126	126 × 126	56 × 126	126 × 126
FOV, mm^2	222 × 222	222 × 222	99 × 222	222 × 222
In-plane resolution, mm	1.8 × 1.8	1.8 × 1.8	1.8 × 1.8	1.8 × 1.8
No. slices	24	24	24	24
Slice thickness, mm	3	3	3	3
Pixel bandwidth, Hz/pixel	1526	863	1526	1526
Acquisition time	05:42	05:48	05:48	05:46

ss-EPI indicates single-shot echo planar imaging; sTX-EPI, selective excitation–reduced field of view echo planar imaging; rs-EPI, readout-segmented echo planar imaging; iShim-EPI, single-shot echo planar imaging with slice-by-slice shimming; FOV, field of view; DWI, diffusion-weighted imaging.

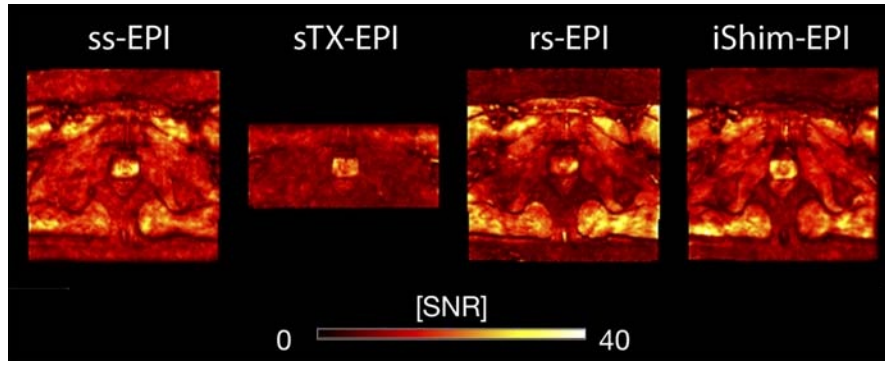

FIGURE 1. Voxel-wise SNR maps for diffusion sequences of a 27-year-old study participant with a body mass index of 24.6 kg/m^2. Diffusion imaging data and corresponding noise data were postprocessed individually, yielding SNR maps on a voxel-wise basis. Signal-to-noise ratio maps for ss-EPI, sTX-EPI, rs-EPI, and iShim-EPI are shown. Signal-to-noise ratio values are color-coded from 0 (black) to 40 (yellow). Figure 1 can be viewed online in color at www.investigativeradiology.com.

Subsequently, a third reader placed region of interests (ROIs) in the peripheral zone as well as within the left and right transitional zone of the prostate. Corresponding mean SNR values in the ROI were extracted, resulting in 1 SNR value for each ROI. Finally, the ROIs located within the left and right transitional zone have been averaged. Thus, SNR values for the peripheral as well as the transitional zone were obtained for each study participant. An example of an SNR map for all DWI sequences is presented in Figure 1.

ADC Measurements and Analysis

For the evaluation of ADC values, ROIs of a fixed size were placed in the left and right peripheral zone as well as in the left and right transitional zone. The mean ADC value was extracted for each ROI. Apparent diffusion coefficient values for the left and right peripheral zone as well as for the left and right transitional zone have been averaged for further analysis.

Geometric Distortion

Quantitative image analysis of geometric distortion was assessed by measuring the diameter of the prostate on b-1000 DWIs and on TSE-T2W images from left to right and from anterior to posterior at the level of the verumontanum (Supplementary Figure 1, Supplemental Digital Content 1, http://links.lww.com/RLI/A359). Differences in diameter between DWI and TSE-T2W images were assessed. Values measured on TSE-T2W images were used as the standard of reference for the definition of anatomic borders. Measurements were conducted using a free digital imaging and communication in medicine viewer (Osirix; version 5.9; The OsiriX Foundation, Geneva, Switzerland).

Statistical Analysis

Interreader agreements for all qualitative image features were assessed using the intraclass correlation coefficient (ICC). An ICC of 0.75 to 1.00 indicated excellent, 0.60 to 0.74 good, 0.40 to 0.59 fair, and less than 0.4 poor agreement.[22] Wilcoxon rank sum tests with Benjamini-Hochberg correction for multiple comparisons were used to detect significant differences in qualitative image features between ss-EPI, rs-EPI, sTX-EPI, and iShim-EPI. Regarding SNR and ADC, analysis of variance (ANOVA) was performed to evaluate potential group interactions with respect to measured SNR and ADC values within the peripheral and transitional zone of the prostate. Post hoc paired-sample *t* tests were performed to identify potential differences in SNR and ADC between each pair of diffusion sequences. Friedman tests were used to detect significant differences in quantitative analysis of geometric distortion. All statistical analyses were performed using SPSS (IBM SPSS Statistics 22; SPSS Inc, Chicago, IL) and R (v3.3.1; The R Foundation for Statistical Software, Vienna, Austria). A (corrected) $P < 0.05$ was considered statistically significant. All tests were 2-tailed.

RESULTS

Qualitative Analysis

Interreader agreement for the 4 different DWI sequences was good for resolution (ICC, 0.712; 95% confidence interval [CI], 0.427–0.852), demarcation of the prostate capsule (ICC, 0.718; 95% CI, 0.473–0.850), the influence of artifacts on image quality (ICC, 0.749; 95% CI, 0.528–0.867), and excellent for zonal anatomy (ICC, 0.790; 95% CI, 0.450–0.905), geometric distortion (ICC, 0.821; 95% CI, 0.662–0.906), the influence of artifacts on the diagnostic performance (ICC, 0.780; 95% CI, 0.584–0.883), overall image quality (ICC, 0.792; 95% CI, 0.586–0.893), and in judging whether the DWI sequence was diagnostic (ICC, 0.777; 95% CI, 0.581–0.882).

There were significant differences in the qualitative feature "resolution" between ss-EPI and rs-EPI ($P = 0.031$), between ss-EPI and sTX-EPI ($P = 0.046$), between iShim-EPI and rs-EPI ($P = 0.031$), and between iShim-EPI and sTX-EPI ($P = 0.047$) (Fig. 2). No significant differences were found in demarcation of the prostate capsule, zonal anatomy, geometric distortion, the influence of artifacts on image quality, and on diagnostic evaluation between these sequences ($P = 0.064$–1).

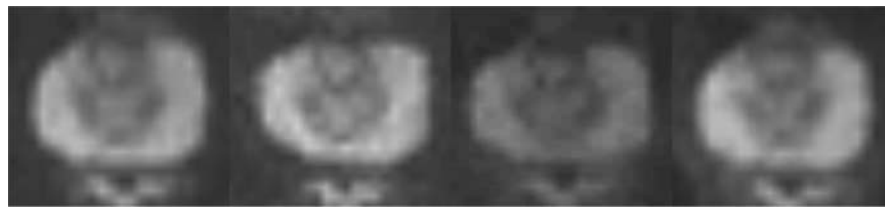

FIGURE 2. Example of differences in the qualitative feature "resolution" between different b-1000 DWI in the same patient. ss-EPI, rs-EPI, sTX-EPI, and iShim-EPI (from left to right) were rated with a 5, 4, 3, and 5, respectively, by reader 1 and 4, 4, 3, and 5, respectively, by reader 2 on a 5-point Likert scale (1, poor; 2, below average; 3, average; 4, above average; 5, excellent).

TABLE 2. Results of Conventional Reading (Likert Score ± Standard Deviation), Numbers of Artifacts, Diagnostic Sequences, and Intraclass Correlation Coefficient

		Reader 1				Reader 2				
		ss-EPI	rs-EPI	sTX-EPI	iShim-EPI	ss-EPI	rs-EPI	sTX-EPI	iShim-EPI	ICC
Scores	Resolution	4.2 ± 0.6	3.2 ± 0.9	3.2 ± 0.9	4.2 ± 0.9	4.3 ± 0.7	4.4 ± 0.8	3.3 ± 1.3	4.5 ± 1.0	0.712
	Capsule demarcation	4.5 ± 0.7	4 ± 0.8	3.9 ± 0.7	4.3 ± 0.9	4.6 ± 1.0	4.4 ± 0.7	3.9 ± 1.0	4.5 ± 0.7	0.718
	Zonal anatomy	3.8 ± 0.8	3.6 ± 1.1	3.2 ± 1.0	3.8 ± 0.9	4.3 ± 1.1	4.4 ± 1.1	3.4 ± 1.3	4.4 ± 1.1	0.790
	Geometric distortion	1.3 ± 0.7	1.4 ± 0.5	1.6 ± 0.7	1.4 ± 1.0	1.5 ± 1.3	1.3 ± 0.7	1.6 ± 0.7	1.5 ± 1.0	0.821
	Artifacts influencing image quality	2.0 ± 0.8	1.8 ± 4.1	3.2 ± 0.9	2.0 ± 1.2	1.7 ± 1.1	1.8 ± 1.3	2.7 ± 1.2	2.2 ± 1.5	0.749
	Artifacts influencing diagnostic evaluation	1.4 ± 1.0	1.4 ± 1.1	2.1 ± 1.1	1.4 ± 1.0	1.3 ± 0.9	1.4 ± 1.0	2.3 ± 1.3	1.8 ± 1.7	0.780
	Overall image quality	3.9 ± 0.9	3.5 ± 1.1	3.1 ± 0.7	4.0 ± 0.8	4.5 ± 0.7	4.2 ± 1.0	3.0 ± 1.2	4.2 ± 1.2	0.792
Artifacts	Total number	8	4	10	6	5	4	8	5	
Diagnostic	Yes	9	9	7	9	10	10	8	9	
	No	1	1	3	1	0	0	2	1	

ss-EPI indicates single-shot echo planar imaging; sTX-EPI, selective excitation–reduced field of view echo planar imaging; rs-EPI, readout-segmented echo planar imaging; iShim-EPI, single-shot echo planar imaging with slice-by-slice shimming.

Furthermore, there were no significant differences in any of the qualitative features between ss-EPI and iShim-EPI (P = 0.5–1) and between rs-EPI and sTX-EPI (P = 0.3–1).

Overall image quality was rated highest for iShim-EPI by reader 1 (4.0, SD ± 0.8) and for ss-EPI by reader 2 (4.5, SD ± 0.7). However, the differences between iShim-EPI and ss-EPI compared with the other DWI sequences were not significant regarding overall image quality for neither reader (P = 0.092–0.396 and P = 0.092–0.773, respectively). Selective excitation–reduced FOV EPI had the lowest score for both readers (3.1, SD ± 0.7 and 3.0, SD ± 1.2, respectively) with the highest number of artifacts (n = 10 and 8), the highest influence of artifacts on the image quality (3.2, SD ± 0.9 and 2.7, SD ± 1.2, respectively), and on the diagnostic performance (2.1, SD ± 1.1 and 2.3, SD ± 1.3, respectively) as well as the highest number of not diagnostic sequences (n = 3 and 2). These differences, however, were not statistically significant. Results are summarized in Table 2.

On a side-by-side comparison, the ss-EPI sequence was most frequently chosen by both readers (in n = 7 of 10 study participants) in terms of overall preference. Prototype single-shot technique applying slice-specific shimming EPI was preferred in n = 3 of 10 study participants by both readers. An example of all 4 DWI sequences is presented side-by-side in Figure 3.

Quantitative Analysis

Signal-to-noise ratio (mean ± SD for the peripheral/transitional zone within the prostate) was 30.24 ± 15.44/15.19 ± 4.32 for ss-EPI, 14.96 ± 2.41/10.93 ± 1.86 for sTX-EPI, 20.52 ± 4.72/13.29 ± 4.74 for rs-EPI, and 28.13 ± 8.21/14.73 ± 2.70 for iShim-EPI, respectively.

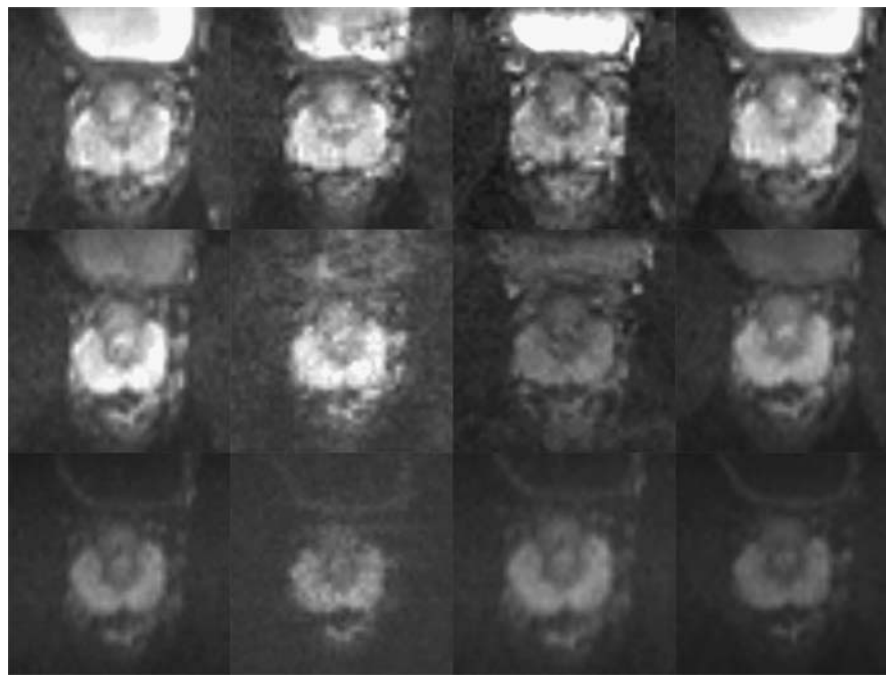

FIGURE 3. Diffusion-weighted imaging of a 26-year-old study participant with a body mass index of 24.7 kg/m^2. First column, ss-EPI; second column, rs-EPI; third column, sTX-EPI; and fourth column, iShim-EPI with b-values of 100, 500, and 1000 s/mm^2 (from the top to the bottom).

TABLE 3. Signal-to-Noise Ratio Analysis

	Peripheral Zone				Transitional Zone			
	SNR	*t*	*P* (Uncorrected)	*P* (Corrected)	SNR	*t*	*P* (Uncorrected)	*P* (Corrected)
ss-EPI vs sTX-EPI	30.24 ± 15.44 vs 14.96 ± 2.41	2.969	*0.018*	0.215	15.19 ± 4.32 vs 10.93 ± 1.86	2.336	*0.048*	0.573
ss-EPI vs rs-EPI	30.24 ± 15.44 vs 20.52 ± 4.72	1.837	0.103	1.242	15.19 ± 4.32 vs 13.29 ± 4.74	0.928	0.381	1.000
ss-EPI vs iShim-EPI	30.24 ± 15.44 vs 28.13 ± 8.21	0.413	0.691	1.000	15.19 ± 4.32 vs 14.73 ± 2.70	0.363	0.726	1.000
sTX-EPI vs rs-EPI	14.96 ± 2.41 vs 20.52 ± 4.72	−3.607	*0.007*	0.083	10.93 ± 1.86 vs 13.29 ± 4.74	−1.640	0.140	1.000
sTX-EPI vs iShim-EPI	14.96 ± 2.41 vs 28.13 ± 8.21	−4.851	*0.001*	*0.015*	10.93 ± 1.86 vs 14.73 ± 2.70	−2.853	*0.021*	0.256
rs-EPI vs iShim-EPI	20.52 ± 4.72 vs 28.13 ± 8.21	−3.520	*0.008*	0.094	13.29 ± 4.74 vs 14.73 ± 2.70	−0.730	0.486	1.000

To evaluate potential differences between pairs of sequences in SNR within the peripheral and transitional zone of the prostate, post hoc paired-sample *t* tests were performed. Corresponding *P* values are given uncorrected as well as corrected for multiple comparisons (Benjamini-Hochberg procedure, n = 12 to account for all performed paired-sample *t* tests). Italics indicate *P* values < 0.05.

ss-EPI indicates single-shot echo planar imaging; sTX-EPI, selective excitation–reduced field of view echo planar imaging; rs-EPI, readout-segmented echo planar imaging; iShim-EPI, single-shot echo planar imaging with slice-by-slice shimming.

Regarding SNR, ANOVA yielded a statistically significant group effect in the peripheral zone ($F = 0.743$, $P = 0.0151$, all given P values corrected for multiple comparisons) but not in the transitional zone ($F = 2.258$, $P = 0.201$). Post hoc paired-sample t tests revealed lower SNR in the peripheral zone for sTX-EPI compared with iShim-EPI ($t = 4.851$; $P = 0.015$). The sTX-EPI showed a trend toward lower SNR in the peripheral zone compared with ss-EPI and rs-EPI as well as lower SNR in the transitional zone compared with ss-EPI and iShim-EPI. However, significance was lost after correction for multiple comparisons (see Table 3 for detailed presentation of SNR results).

Apparent diffusion coefficient (mean ± SD for the peripheral/transitional zone within the prostate) was 1165.05 ± 115.64/1066.64 ± 188.15 for ss-EPI, 1244.40 ± 89.95/1261.47 ± 179.23 for rs-EPI, 1002.94 ± 83.51/874.50 ± 200.72 for sTX-EPI, and 1133.37 ± 141.17/1075.21 ± 162.75 for iShim-EPI, respectively. The ANOVA showed a statistically significant group effect in the peripheral zone ($F = 8.355$, $P = 0.0024$, also, all given P values corrected for multiple comparisons) and the transitional zone ($F = 7.437$, $P = 0.001$). Post hoc paired-sample t tests revealed significant lower ADC values for the peripheral zone in the sTX-EPI compared with the ss-EPI ($P = 0.013$) and the rs-EPI ($P = 0.0012$). Furthermore, the post hoc paired-sample t tests revealed significant lower ADC-values for the transitional zone in the sTX-EPI compared with the rs-EPI ($P = 0.0021$). There were no significant differences between all other DWI sequences in the peripheral and transitional zone.

There were no statistically significant differences in left to right and anterior to posterior diameter of the prostate between all 4 different DWI sequences and the TSE-T2W sequences ($P = 0.196$) with a median diameter difference of −0.5 mm (interquartile range [IQR], −0.7 to 0.8 mm) and −0.6 mm (IQR, −1.7 to 1.1 mm) for the ss-EPI, 0.2 mm (IQR, −1.6 to 1.3 mm) and 0.3 mm (IQR, −0.5 to 1.1 mm) for the rs-EPI, 1.6 mm (IQR, 0.4 to 3.9 mm) and 1.6 (IQR, −0.9 to 2.3 mm) for the sTX-EPI, and 0.6 mm (IQR, 1.7 to 1.1 mm) and 0 (IQR, −1.4 to 1.3 mm) for the iShim-EPI, respectively.

DISCUSSION

Our study investigates 4 modern DWI sequences for MRI of the prostate. A tendency toward superior image quality for ss-EPI and iShim-EPI sequences was seen, however, statistical significance of these differences was reached in only 1 evaluated feature of image quality ("resolution"). In a side-by-side comparison of the 4 DWI sequences, both readers preferred ss-EPI and iShim-EPI over rs-EPI and sTX-EPI. The subjective preference of these 2 DWI sequences was paralleled with the findings of the SNR analysis, in which ss-EPI and iShim-EPI showed a trend toward higher SNR compared with rs-EPI and sTX-EPI in the peripheral and transitional zone. The higher SNR of the single-shot full-FOV techniques is expected due to their higher sampling efficiency.

Two of the 4 tested sequences, rs-EPI and sTX-EPI, have been compared in a recent study[15] and have shown comparable image quality with higher geometric distortion in the sTX-EPI sequence. In our study, the geometric distortion in all tested sequences was not significantly different, possibly due to acquisition without an endorectal coil in our study as compared with the previous study. Especially, the sTX-EPI seemed to be prone to susceptibility artifacts at the coil-prostate border when acquired using an endorectal coil. Another difference as opposed to the study by Barth et al[15] was the focus on comparable acquisition time between all 4 tested sequences in our study. While previously conducted studies demonstrated improved image quality and less geometric distortion for rs-EPI in various parts of the body[23–27] and in the prostate[28] as compared with ss-EPI, we could not demonstrate superiority of rs-EPI imaging versus ss-EPI. It seems that the moderate spatial resolution used in our study in combination with the high receiver bandwidth and well-adjusted B_0-field did not result in severe T2* signal

decay during the EPI readout train and therefore lead to high image quality that could not be improved further by the rs-EPI or sTX-EPI techniques. Readout-segmented multishot EPI and sTX-EPI may demonstrate their full potential for higher spatial in-plane resolution that would require very long echo-trains when using single-shot full-FOV techniques. By keeping the acquisition time for all 4 tested sequences comparable, the rs-EPI might not have been optimized to its fullest potential; however, we focused on keeping the acquisition time for all sequences reasonable considering a clinical application. Contrary to our study, previously published studies by Thierfelder et al[12] and Rosenkrantz et al[16] showed improved image quality and reduction of artifacts for sTX-EPI sequences in the prostate as compared with ss-EPI. However, in these studies, the acquisition time for the ss-EPI was either distinctly shorter compared with the sTX-EPI[12] or both acquisition times were markedly longer as compared with our study.[16] Also, TE for ss-EPI was considerably longer and in-plane resolution slightly higher than in our sequences, possibly leading to a lower SNR as compared with our sequences. The slightly but significantly lower ADC values measured in the peripheral zone and transition zone of the sTX-EPI sequence might have been caused by the differences in image quality or possible artifacts altering the measurements. The differences of ADC values measured in our study lie within reported coefficients of variation in ADC in abdominal organs between MRI scanners of different vendors.[29] Nevertheless, the possibility of differences in ADC measurements between different DWI techniques should be considered in case quantitative measures will be included in updated versions of guidelines on interpreting prostate MRI. Another reason for the different outcome compared with the study by Thierfelder et al might be the different study population: in our study, young and healthy volunteers were examined with possibly less air in the rectum than in a typical patient population and therefore less pronounced problems with artifacts and distortion at the rectum-prostate interface.

The EPI sequence with integrated 2D slice-by-slice shimming (iShim-EPI) showed improved image quality compared with rs-EPI and sTX-EPI and similar image quality compared with ss-EPI. This sequence has recently been evaluated and compared with ss-EPI in head and neck[13,30] and in whole-body applications.[14] In both of these studies, iShim-EPI showed less spatial distortion and higher image quality in the neck area. In our study, probably due to evaluation of a less artifact-prone anatomical region, these benefits in reduced geometric distortion were not present. Altogether, the reduced geometric distortion and proposed advantage in artifact reduction of rs-EPI, sTX-EPI, and iShim-EPI as opposed to ss-EPI could not be demonstrated in MRI of the prostate of healthy volunteers. They may, however, be able to show their potential in reducing artifacts and geometric distortion in situations where ss-EPI is prone to artifacts, such as in the presence of air in the rectum during prostate MRI or in patient with hip implants.[31]

Our study has limitations. First, we investigated young and healthy volunteers instead of patients with a clinical suspicion of prostate cancer. Volunteers were chosen for this study in to compare different DWI sequences in a homogeneous population. This population had a normal body mass index and normal prostate zonal anatomy and does not reflect the typical patient population undergoing prostate MRI for suspected prostate cancer. However, as each DWI sequence was acquired twice to calculate voxel-by-voxel SNR, the acquisition time for the DWI comparison was substantial and it would not have been feasible to perform this study in clinical practice on patients. Second, the sample size was small, but in the typical order for volunteer studies of this type. Third, due to the choice of the study population, effects of the different DWI sequences on diagnostic accuracy could not be assessed. Fourth, the highest b-value acquired in our study subject was b = 1000 s/mm^2. Because the aim of the study was to compare image quality and not lesion depiction, we did not acquire higher b-values, which might be helpful for diagnostic purposes. However, the high b-value images (b ≥ 1400 s/mm^2) may be calculated from the acquired b-values in concordance with PI-RADS v2 guidelines.

In conclusion, ss-EPI and iShim-EPI showed a tendency toward better image quality and SNR compared with rs-EPI and sTX-EPI in prostate MRI of healthy volunteers. No significant differences in geometric distortion were seen between all 4 DWI sequences.

REFERENCES

1. Radiology ACo 2015; Pages. Accessed at http://www.acr.org/~/media/ACR/Documents/PDF/QualitySafety/Resources/PIRADS/PIRADS%20V2.pdf/. Accessed August 18, 2016.
2. Scheenen TW, Rosenkrantz AB, Haider MA, et al. Multiparametric magnetic resonance imaging in prostate cancer management: current status and future perspectives. *Invest Radiol*. 2015;50:594–600.
3. Weinreb JC, Barentsz JO, Choyke PL, et al. PI-RADS prostate imaging - reporting and data system: 2015, version 2. *Eur Urol*. 2016;69:16–40.
4. Donati OF, Mazaheri Y, Afaq A, et al. Prostate cancer aggressiveness: assessment with whole-lesion histogram analysis of the apparent diffusion coefficient. *Radiology*. 2014;271:143–152.
5. Ueno Y, Takahashi S, Kitajima K, et al. Computed diffusion-weighted imaging using 3-T magnetic resonance imaging for prostate cancer diagnosis. *Eur Radiol*. 2013;23:3509–3516.
6. Vargas HA, Akin O, Franiel T, et al. Diffusion-weighted endorectal MR imaging at 3 T for prostate cancer: tumor detection and assessment of aggressiveness. *Radiology*. 2011;259:775–784.
7. Akisik FM, Sandrasegaran K, Aisen AM, et al. Abdominal MR imaging at 3.0 T. *Radiographics*. 2007;27:1433–1444; discussion 62–64.
8. Farzaneh F, Riederer SJ, Pelc NJ. Analysis of T2 limitations and off-resonance effects on spatial resolution and artifacts in echo-planar imaging. *Magn Reson Med*. 1990;14:123–139.
9. Lee VS, Hecht EM, Taouli B, et al. Body and cardiovascular MR imaging at 3.0 T. *Radiology*. 2007;244:692–705.
10. Porter DA, Heidemann RM. High resolution diffusion-weighted imaging using readout-segmented echo-planar imaging, parallel imaging and a two-dimensional navigator-based reacquisition. *Magn Reson Med*. 2009;62:468–475.
11. Mathias Blasche MPR, MD, Mathias Lichy MD. *TimTX TrueShape and syngo ZOOMit technical and practical aspects MAGNETOM Flash*. 2012;10.
12. Thierfelder KM, Scherr MK, Notohamiprodjo M, et al. Diffusion-weighted MRI of the prostate: advantages of Zoomed EPI with parallel-transmit-accelerated 2D-selective excitation imaging. *Eur Radiol*. 2014;24:3233–3241.
13. Walter SS, Liu W, Stemmer A, et al. Combination of integrated dynamic shimming and readout-segmented echo planar imaging for diffusion weighted MRI of the head and neck region at 3Tesla. *Magn Reson Imaging*. 2017;42:32–36.
14. Zhang H, Xue H, Alto S, et al. Integrated shimming improves lesion detection in whole-body diffusion-weighted examinations of patients with plasma disorder at 3 T. *Invest Radiol*. 2016;51:297–305.
15. Barth BK, Cornelius A, Nanz D, et al. Diffusion-weighted imaging of the prostate: image quality and geometric distortion of readout-segmented versus selective-excitation accelerated acquisitions. *Invest Radiol*. 2015;50:785–791.
16. Rosenkrantz AB, Chandarana H, Pfeuffer J, et al. Zoomed echo-planar imaging using parallel transmission: impact on image quality of diffusion-weighted imaging of the prostate at 3 T. *Abdom Imaging*. 2015;40:120–126.
17. Nketiah G, Selnaes KM, Sandsmark E, et al. Geometric distortion correction in prostate diffusion-weighted MRI and its effect on quantitative apparent diffusion coefficient analysis. *Magn Reson Med*. 2017.
18. Weygand J, Fuller CD, Ibbott GS, et al. Spatial precision in magnetic resonance imaging-guided radiation therapy: the role of geometric distortion. *Int J Radiat Oncol Biol Phys*. 2016;95:1304–1316.
19. Reeder SB, Wintersperger BJ, Dietrich O, et al. Practical approaches to the evaluation of signal-to-noise ratio performance with parallel imaging: application with cardiac imaging and a 32-channel cardiac coil. *Magn Reson Med*. 2005;54:748–754.
20. Filli L, Piccirelli M, Kenkel D, et al. Simultaneous multislice echo planar imaging with blipped controlled aliasing in parallel imaging results in higher acceleration: a promising technique for accelerated diffusion tensor imaging of skeletal muscle. *Invest Radiol*. 2015;50:456–463.
21. Manoliu A, Ho M, Piccirelli M, et al. Simultaneous multislice readout-segmented echo planar imaging for accelerated diffusion tensor imaging of the mandibular nerve: a feasibility study. *J Magn Reson Imaging*. 2017;46:663–677.
22. Hallgren KA. Computing inter-rater reliability for observational data: an overview and tutorial. *Tutor Quant Methods Psychol*. 2012;8:23–34.
23. Tokoro H, Fujinaga Y, Ohya A, et al. Usefulness of free-breathing readout-segmented echo-planar imaging (RESOLVE) for detection of malignant liver tumors: comparison with single-shot echo-planar imaging (SS-EPI). *Eur J Radiol*. 2014;83:1728–1733.

24. Wisner DJ, Rogers N, Deshpande VS, et al. High-resolution diffusion-weighted imaging for the separation of benign from malignant BI-RADS 4/5 lesions found on breast MRI at 3 T. *J Magn Reson Imaging*. 2014;40:674–681.
25. Wu CJ, Wang Q, Zhang J, et al. Readout-segmented echo-planar imaging in diffusion-weighted imaging of the kidney: comparison with single-shot echo-planar imaging in image quality. *Abdom Radiol (NY)*. 2016;41:100–108.
26. Xia CC, Liu X, Peng WL, et al. Readout-segmented echo-planar imaging improves the image quality of diffusion-weighted MR imaging in rectal cancer: Comparison with single-shot echo-planar diffusion-weighted sequences. *Eur J Radiol*. 2016;85:1818–1823.
27. Yeom KW, Holdsworth SJ, Van AT, et al. Comparison of readout-segmented echo-planar imaging (EPI) and single-shot EPI in clinical application of diffusion-weighted imaging of the pediatric brain. *AJR Am J Roentgenol*. 2013;200:W437–W443.
28. Li L, Wang L, Deng M, et al. Feasibility study of 3-T DWI of the prostate: readout-segmented versus single-shot echo-planar imaging. *AJR Am J Roentgenol*. 2015; 205:70–76.
29. Donati OF, Chong D, Nanz D, et al. Diffusion-weighted MR imaging of upper abdominal organs: field strength and intervendor variability of apparent diffusion coefficients. *Radiology*. 2014;270:454–463.
30. Gatidis S, Graf H, Weiss J, et al. Diffusion-weighted echo planar MR imaging of the neck at 3 T using integrated shimming: comparison of MR sequence techniques for reducing artifacts caused by magnetic-field inhomogeneities. *MAGMA*. 2017;30:57–63.
31. Rosenkrantz AB, Taneja SS. Use of reduced field-of-view acquisition to improve prostate cancer visualization on diffusion-weighted magnetic resonance imaging in the presence of hip implants: report of 2 cases. *Curr Probl Diagn Radiol*. 2017.